Persistent M2 phase in strongly strained (011)-oriented grains in VO_2 films grown on sapphire (001) in reactive sputtering

Kohei Matsuoka[1)], Kunio Okimura,[1,a)] Nurul Hanis Azhan[2)],

Mustapha Zaghrioui,[3)] and Joe Sakai [4)]

[1] *Graduate School of Engineering, Tokai University, Hiratsuka 259-1292, Japan*

[2] *Electrical Engineering Section, Universiti Kuala Lumpur British Malaysian Institute, 53100 Gombak, Selangor, Malaysia*

[3] *Laboratoire GREMAN CNRS-UMR 7347, IUT de BLOIS, 15, rue de la Chocolaterie, C. S. 32903, 41029 Blois Cedex, France*

[4] *Institut Català de Nanociència I Nanotecnologia (ICN2),ICN2 Building, UAB Campus 08193 Bellaterra, Spain*

Abstract

We report on first observation of persistent M2 phase in strongly strained (011)-oriented grains in VO_2 films grown on Al_2O_3 (001) substrates by means of conventional rf reactive sputtering under adequate deposition conditions. Spatially resolved micro-Raman clearly showed that (011)-oriented large crystalline grains with c_R-axis parallel to the substrate underwent appearance of M2 phase over a wide temperature range of 30°C. Close correlation of the appearance range of M2 phase with in-plane tensile stress of (011)-oriented grains was revealed by x-ray diffraction (XRD). We demonstrated a phase diagram for M1, M2 and R phases in relation between the stress of (011)-oriented grains and the temperature. It was shown that (011)-oriented μm-sized long grains play a crucial role for emerging structural phase transition (SPT) via a M2 phase even in a film grown on Al_2O_3 (001), which is ordinally served for (020)-oriented VO_2 growth. The results shown here will contribute to make clear the condition for obtaining VO_2 films with appearance of M2 phase in their SPT process.

[a)]Electronic mail: okifn@keyaki.cc.u-tokai.ac.jp

I. INTRODUCTION

A strongly correlated oxide, vanadium dioxide (VO_2), has been collecting wide variety of interests in views of engineering applications utilizing the drastic changes of physical properties concomitant with its insulator-metal transition (IMT) phenomenon.[1-3] There have been several decades devoted for clarifying correlation between the IMT and the structural phase transition (SPT) in order to realize desired properties of VO_2.[4,5] In addition, recent growing interests for application of the IMT to electrical, optical and thermal devices request the controllability of IMT in VO_2 thin films.[6-11] Newly launching attempts to apply the IMT for neuromorphic computing and terahertz switching require further understanding of physics of thin film VO_2.[3, 12-15]

So far, lots of studies on VO_2 single crystals and VO_2 films suggested that the distance of V atoms along c_R-axis (in the high-temperature tetragonal phase, R phase) determines the IMT temperature.[16-18] VO_2 films grown on TiO_2 (001) substrates, in which IMT occurs at room temperature (around 300 K), contribute to broaden the applicability of VO_2 films.[19] However, there is still a remaining dispute on the appearance of intermediate phase in the SPT pathway from monoclinic M1 phase to tetragonal R phase, especially in VO_2 thin films.[20-25] Conditions for appearance of the intermediate M2 phase with monoclinic symmetry have been minutely investigated by using VO_2 single-crystalline nanorods (usually called nanobeams) by many authors.[26-31] Phase diagrams as functions of temperature and stress along c_R-axis were shown for SPT of single-crystalline VO_2.[28,30] As for VO_2 films grown on various substrates, appearance of M2 phase strongly depends on deposition conditions, which affect the stress on the VO_2 films.[32,33] Polycrystalline VO_2 films have grain boundaries even though they are composed of highly oriented grains, giving complicated situation of stress state acting on the grains.[33,34] In addition, coexistence of V_nO_{2n-1} and V_nO_{2n+1} phases different from

stoichiometric VO_2 invites difficulties for considering the relation between the stress and the M2 phase.[35,36]

Al_2O_3 (001) substrates are frequently utilized for the growth of VO_2 films in which b_M-axis (in the low-temperature monoclinic M1 phase) oriented VO_2 grains are grown with in-plane three directions based on the lattice matching between hexagonal plane of Al_2O_3 (001) and a_M-c_M plane of VO_2.[37] Since the c_R-axis (a_M-axis) is parallel to the Al_2O_3 (001) plane, stress on the VO_2 film acts on the V-V chains, giving possibilities of inducing M2 phase if strong tensile stress is remained in the film. Thery *et al*. reported the SPT via a M2 phase in relatively thin VO_2 films on Al_2O_3 (001) deposited by electron-beam evaporation due to the tensile stress, which originates in the difference of thermal expansion coefficient between VO_2 and Al_2O_3.[32] We also reported that the SPT with intermediate M2 phase was observed in the VO_2 film on Al_2O_3 (001) deposited by biased reactive sputtering.[36,38] The films we obtained were dominated by (011)-oriented large crystalline domains, which underwent SPT with M2 phase. The temperature range of appearance of M2 phase was as narrow as 10 - 15°C. Based on these studies, the fact that tensile stress on c_R-axis induces SPT with M2 phase even in thin films was observed. However, the correlation between the stress strength and the temperature range of appearance of M2 phase was unclear due to the presence of disorder and the grain boundaries in the VO_2 film on the substrate. Grain boundaries reduce stress on the VO_2 grains, specially in the case of VO_2 on Al_2O_3 (001), because of the restricted small grain sizes. Thus, it is highly desired to observe the effect of tensile stress on the appearance of M2 phase directly in the VO_2 film on Al_2O_3 (001).

In this article, we show the case in which (011)-oriented long plate-like grains were grown on Al_2O_3 (001) substrates under adequate deposition conditions in conventional reactive sputtering. We demonstrate that the (011)-oriented grains underwent SPT with

persistent M2 phase over 30°C through the micro-Raman observations for the particular grains. A phase diagram for M1, M2, and R phases in relation between the stress on the (011)-oriented grains and the temperature is shown. We discuss the correlation of appearance of M2 phase in VO_2 films grown on Al_2O_3 (001).

II. EXPERIMENTAL METHODS

VO_2 films were deposited by conventional radio frequency (rf) magnetron sputtering. In this study, we did not utilize substrate biasing that we introduced before.[36] Polished Al_2O_3 (001) was used as the substrate and was placed at the center position on the lower electrode. Temperature of the substrate and the rf power fed to the metal vanadium (99.9%) target with diameter of 100 mm were 450°C and 200 W, respectively. Flow rates of Ar and O_2 gases were 38 and 1 sccm, respectively. Total pressure of Ar and O_2 gases was 0.5 Pa. We varied deposition period as 10, 20, and 30 min.

Crystalline structures of VO_2 films were analyzed by X-ray diffraction (XRD; Philips, X'pert MRD) with CuKα X-ray source (λ = 1.5418 Å). Temperature-dependent Micro-Raman measurements were also performed to investigate SPT at a particular crystalline region. The Raman setup utilizes 514 nm Ar ion laser with a power of 0.5 mW as the light source. The incident laser light was focused by a $\times$50 lens (0.50NA) which realizes the spatial resolution of around 2 μm.[39] Reflex device (Renishaw, inVia) and a temperature controller (Linkam, THMS 600) were introduced for temperature-controlled Raman measurements. Field emission scanning electron microscopy (FE-SEM; Hitachi, S-4800) was used for observing both the surface and cross-sectional morphologies of the VO_2 films. Atomic force microscopy (AFM; Shimadzu, SPM-9700) was also utilized to observe crystalline growth aspects and minute surface roughness. Electron probe microscopy analysis (EPMA; Shimadzu, EPMA-1610) was

introduced to investigate spatial difference of atomic concentration. Resistance changes against temperature were measured by two electrical probe tips, which are made of tungsten carbide (WC). Film thickness was evaluated by cross-sectional SEM images.

III. RESULTS AND DISCUSSION

Figure 1 shows XRDs for VO_2 films deposited for different periods of 10, 20 and 30 min. We named these samples as S1 (10 min), S2 (20 min) and S3 (30 min). Film thicknesses were 100, 290, and 340 nm for S1, S2, and S3, respectively. In all samples, we see diffraction from VO_2 (020) plane at around $2\theta = 39.8°$, whose FWHM of rocking curves were 0.09°, 0.14°, and 0.11° for S1, S2 and S3, respectively. Growth of (020)-oriented VO_2 films on Al_2O_3 (001) is commonly known in addition to the in-plane three growth directions based on lattice matching between a_M-c_M plane with β angle of 122° and the hexagonal Al_2O_3 (001) plane. Large shift [$2\theta = 39.98°$, $d_{(020)} = 2.255$ Å against bulk $2\theta = 39.83°$, $d_{(020)} = 2.263$ Å] of the XRD peak position for (020) in the sample S1 means occurrence of strong in-plane tensile stress, which is basically caused by the thermal stress. As suggested by many researchers, large difference of thermal expansion coefficient between VO_2 (29.7×10^{-6} /K along c_R-axis in tetragonal phase) and Al_2O_3 (5.0×10^{-6} /K) results in large tensile stress.[32] Simple estimation of the in-plane thermal stress of a VO_2 film with c_R-axis parallel to the Al_2O_3 (001) substrate gives -1.10 GPa at a temperature of 70°C for the deposition temperature of 450°C when we use Young's modulus E of 140 GPa. Thery *et al.* showed relaxation of in-plane tensile strain with increase of VO_2 film thickness deposited by electron-beam evaporation method, where residual stress is dominated by thermal stress and its relaxation occurred with increasing thickness.[32] However, in our experiment using reactive sputtering, where

energetic ions assist crystalline growth, (011)-oriented VO_2 growth also appeared at deposition periods of 20 and 30 min as shown in Fig. 1.

We see strong diffraction peaks from VO_2 (011) at around $2\theta = 27.9°$ for S2 and S3, in Fig. 1(b). As shown in Fig. 1(c), rocking curves for (011) plane showed small values of FWHM of 0.13° and 0.10° for S2 and S3, indicating superior orientation of the grains. In addition, higher peak position of (011) of S2 [$2\theta = 27.955°$, $d_{(011)} = 3.1916$ Å, against bulk $2\theta = 27.85°$, $d_{(011)} = 3.2034$ Å] suggested strong in-plane tensile stress on the (011)-oriented grains. The fact that the in-plane tensile stress estimated by the shift of (020) peak was rather relaxed in S2 compared to that of S1 suggested the difference of stress between VO_2(020) and (011) crystalline grains. It is known that the stress in poly-crystalline films differs between crystallite and grain boundaries.[40] We elucidate that the stress of the sample S2 depends on crystallites with different sizes as evidenced later by SEM images. The higher peak position of (011) at $2\theta = 27.955°$ in S2 corresponds to out-of-plane compression ε_z of -0.37%, which is caused by in-plane tensile stress $\sigma_{//}$ based on the elastic-body approximation. We adopted well-known relationship of $\sigma_{//} = -E\varepsilon_z/2v$, where v is Poisson ratio, for deriving the in-plane stress. By using the reported values of E and v of 140 GPa and 0.30,[42,43] tensile stress of 860 MPa was obtained for the (011)-oriented grains. On the other hand, peak position of (011) in S3 was almost in accordance with that of bulk VO_2, suggesting that the stress on the (011)-oriented grains was relaxed in this sample through the increase of film thickness.

Figure 2 shows FE-SEM images of VO_2 films for S1, S2 and S3. Noticeable grains cannot be seen in S1 as shown in Fig. 2 (a), suggesting that the thinnest film is composed of (020)-oriented fine crystalline grains. In Fig. 2 (b), we found μm-sized large crystalline grains in S2 in addition to conventional smaller grains with (020)-orientation. In inset of Fig. 2(b), we show another SEM image that clearly shows the

plate-like crystalline grain with width and length of around 1 μm and 6 μm, respectively. Cross-sectional SEM image for S2 also evidenced the presence of plate-like crystallite in Fig. 2 (c). When we increased deposition time to 30 min in S3, as can be seen in Fig. 2 (d), large crystalline grains with dark contrast were enlarged to more than several tens μm square, although many grain boundaries were present. Such large crystalline grains were confirmed to be corresponding to (011)-oriented VO_2 by area-restricted XRD measurements as shown in FIG. A in the supplementary material. Fig. 2 (e1) shows an AFM image for S2, in which rod-shape crystallites are grown in the fine matrix grains. Height analysis shown in Fig. 2 (e2) evidenced flat surface of the crystallite in contrast to matrix grains with rough surfaces and deep grain boundaries. Based on the results of SEM and AFM images, characteristic μm-sized large crystalline grains in S2 were judged to be attributed to (011)-oriented crystallites. It can be elucidated that with increasing film thickness, (011)-oriented rod-shape crystallites coalesced and resulted in the formation of large grains . Rod-shape crystallites are no longer observed in S3, suggesting the relaxation of in-plane stress on particular direction.

Here, it should be noted that glancing incidence XRD (GI-XRD) showed the diffraction from V_6O_{13} in all samples. V_6O_{13}, which is categorized as one of Sharley phases with V_nO_{2n+1} like V_2O_5, is known to transform to VO_2 by annealing because of its quite low melting temperature of 680°C.[41] We elucidate that the (011)-oriented grains were nucleated and grown from the crystalline nuclei of highly oxidized V_6O_{13} present with (020)-oriented VO_2 fine grains. Agreeing this matter, EPMA mapping images for oxygen (O) concentration in Figs. 2 (f1) and (f2) show that (011)-oriented large grains contain less O compared to the surrounding matrix region.

Figure 3 (a) shows the results of temperature-dependent micro-Raman measurement on particular rod-shape grain in the film S2. Superior crystallinity of the film at room

temperature (20°C) was evidenced by a series of intense peaks corresponding to M1 phase VO_2. Continuation of M1 phase till 65°C was clearly recognized. At 70°C, we recognized the onset of blue shift of the peak at 618 cm^{-1} (V-O stretching mode in M1). A complete shift of the peak to 648 cm^{-1} (V-O stretching mode in M2) was clearly observed at 75°C. Characteristic splitting in the peaks at 220 and 229 cm^{-1} (V-V stretching mode in M2) was also recognized, suggesting that superior crystalline M2 phase VO_2 was formed at this temperature. The M2 phase continued to occur clearly until 100°C and then transformed to R phase thoroughly at 110°C. Structural phase transition from M1 to M2 with such superior crystallinity and persistent M2 phase for a range of over 30°C is the first observation in VO_2 films grown on Al_2O_3 substrates. On the other hand, Fig. 3 (b) shows micro-Raman spectra taken for the matrix region, where several tens nm grains with (020)-orientation were grown. We also recognize superior crystallinity of M1 phase VO_2 at room temperature (20°C), similarly to Fig. 3 (a). It can also be seen that the peak at 618 cm^{-1} showed a blue shift to 648 cm^{-1} at 75°C, indicating appearance of M2 phase. However, characteristic spectra for M2 phase soon disappeared until 85°C.

Figures 3 (c) and (d) show the color plots of temperature-dependence of Raman peak position reproduced from the data shown in Figs. 3 (a) and (b). An abrupt peak shift from 618 to 648 cm^{-1} at 75°C was clearly demonstrated in Fig. 3 (c). On the other hand, appearance of M2 phase was hardly recognized for (020)-oriented area in Fig. 3 (d). In order to evaluate quantitative evolution of M1, M2 and R phases, we calculated intensity of Raman peaks by adopting Lorentzian fittings for both (011) and (020)-oriented grains shown in Figs. 3 (a) and (b). We focused on Raman mode of 619 cm^{-1} for M1 and 648 cm^{-1} for M2 phases as representatives. To represent R phase, which has strong background for a wide wavenumber range [See Figs. 3 (c) and (d)], we integrated

the intensity for 900 – 1100 cm^{-1}, where no Raman mode exists in any phases. Through the curve fittings, it was confirmed that the M2 phase appeared simultaneously with R phase after 65°C in both cases. We show the evolution of each phase for both (011) and (020)-grains in FIG. B in the supplementary material.

Furthermore, we performed micro-Raman measurements for the film S3. In Fig. 3 (e), we recognize the shifted peak at 648 cm^{-1} at temperatures from 75 to 80°C. Also in Fig. 3 (f), we recognize the shifted peak from 75 to 80°C. However, Raman spectra characteristic in M2 phase were weak compared to those appeared in (011)-oriented grain in S2. In our previous paper, we reported the SPT through M2 phase in VO_2 films deposited on Al_2O_3 (001) substrates by using biased reactive sputtering.[36,38] We elucidated that the formation of (011)-oriented large crystalline grains was driven by a high-energy ion irradiation effect on the excess oxygen phases, which act as nuclei for the growth of (011)-oriented large domains. However, appearance of M2 phase was restricted to a narrower temperature range similar to those in Figs. 3 (e) and (f). Thus, we emphasize that the enhanced crystallinity and persistency of M2 phase were firstly demonstrated in this study by taking micro-Raman on the (011)-oriented long grains under high in-plane tensile stress. It is suggested that the appearance of M2 phase in the course of SPT of VO_2 film strongly depends on the aspect of crystalline orientation and grain sizes because they dominate collective effect of stress on particular c_R-axis direction.[42] We elucidate that in a highly-strained (020)-oriented VO_2 film it is difficult to emerge M2 phase over a wide temperature range due to the small grain sizes in which stress effect is relaxed by the grain boundaries. We also show the evolution of Raman peak intensity of each phase for both (011) and (020)-grains of S3 in FIG. B in the supplementary material.

Based on the micro-Raman measurements, we drew the phase diagram for M1, M2 and R phases in relation between the stress on (011)-oriented grains and the temperature, as shown in Fig. 4. As mentioned before, we evaluated the in-plane stress values from the out-of-plane strain obtained by the peak position of (011), assuming elastic-body approximation with Young's modulus and Poisson's ratio of 140 GPa and 0.30. The stress values for (011)-oriented grains for samples S2 and S3 are 860 and 165 MPa, respectively. As the results, it can be seen that increasing tensile stress induces a wider temperature window for M2 phase. High temperature side was extended by the increasing stress, while the lowest temperature side for M2 phase was rather constant at around 70°C. The added datum for the VO_2 film with (011)-oriented large domains was based on the peak position of XRD presented in our previous paper,[36] supporting validity of proposed phase space regardless of difference in the deposition method. The boundary between M2 and R phases obtained by the present study for sample S2 almost corresponds to the extrapolated line based on the result of Park *et al*.[43] The present result, in which the crystalline grain under strong tensile stress of 0.86 GPa shows persistent M2 phase until 100°C, suggested invariant nature of SPT in VO_2. On the other hand, it can be seen that the boundary from M1 to M2 phases obtained by the present study was different from those using VO_2 nanobeams.[28,30,43] SPT from M1 to M2 was observed at almost constant temperature of around 70°C in our study. As shown in Fig. 3 (b), (020)-oriented grains showed the onset of SPT at 70°C, same as the onset of (011)-oriented grains.

Here, we consider the cause for simultaneous onset for appearance of M2 phase for both (011) and (020)-oriented grains. When we discuss the SPT of VO_2, it is necessary to compare lattice length toward c_R direction. Monoclinic M2 phase has been reported to have lattice length of a_{M2} = 9.0664 Å, b_{M2} = 5.797 Å, c_{M2} = 4.5255 Å, β_{M2} = 91.88°,

respectively.[20] Meanwhile, as well known, M1 phase has a_{M1} = 5.753 Å, b_{M1} = 4.526 Å, c_{M1} = 5.383 Å, β_{M1} = 122.6°, respectively and tetragonal rutile phase has a_R = 4.555 Å and c_R = 2.853 Å.[20] Thus, corresponding lattice length of a_{M1}, $2c_R$, and b_{M2} are 5.753, 5.706, and 5.797 Å, respectively. The length would be then compressed by -0.8 % upon M1 to R transition, while it would be tensiled by 0.76 % upon M1 to M2 transition. As Zhang *et al.* suggested, the compression upon M1 to R phase transition induces tensile stress, which can locally stabilize the formation of M2 phase with a large cell length of b_{M2}.[27] Thus, formation of M2 phase follows nucleation of R phase. In addition, the onset of SPT of (011)-oriented grains will be strongly restricted by the surrounding (020)-oriented matrix grains. When VO_2 transforms from M1 to M2 phase, unit cell volume increases by about 0.66% with in-plane enlargement for $2V_{M1} \rightarrow V_{M2}$. Then, SPT of M1 to M2 would be severely restricted by unchanged surrounding matrix. Therefore, we interpret that the (011)-oriented grains revealed SPT from M1 to M2 at temperatures corresponding to that from M1 to R of (020)-grains. Naturally, the SPT of (020) grains from M1 to M2 is simultaneously occurred. As shown in Fig. 3, peak intensity of M2 phase in (020) grains was smaller than that of (011) grains in S2. Therefore, we interpret that simultaneous onset of appearance of M2 phase for both (011) and (020)-oriented grains occurred at a temperature at which SPT from M1 to R phase was initiated. On the other hand, the SPT from M2 to R is accompanied by slight volume decrease of 0.40%, which enables (011)-oriented grains transformation according to the stress-temperature phase diagram.

Kim *et al.* reported that single-crystal VO_2 wires with length over 10 μm grown on r-cut sapphire substrate possess M2 phase which are stable from 19 to 100°C.[44] They expected that thicker wires with greater stress supplied sufficient driving force to nucleate the M2 phase in addition to the effect of substrate-mediated interaction. Thus,

we interpret that the growth of large grains with superior crystallinity is a key issue to emerge persistent M2 phase. Furthermore, the occurrence of M2 phase in VO_2 films on Al_2O_3 (001) substrates was reported by Ji *et al.*[22] They mentioned that the temperature window for M2 phase depends on tensile strain relevant to film thickness. Thus, in the present study, large in-plane tensile stress in (011)-oriented grains in S2 contributes to enlarge the window for M2 phase as shown in Fig. 4.

Finally, we show resistance (R) – temperature (T) characteristics for S1, S2 and S3 films in Fig. 5. Resistance was measured by two probe tips separated by 1 mm. As can be seen, resistance changes more than three orders of magnitude were observed after the onset of IMT in both S2 and S3. Values of transition temperature defined by the peak of $-\mathrm{d}(\log_{10}R)/\mathrm{d}T$ against rising temperature were 77 and 79°C for S2 and S3, higher than that of S1 (75°C). Resistance started to decrease with the onset of SPT at around 70°C in both S2 and S3. As shown in temperature-dependent Raman measurements, R phase increases its domination with accordance to the decrease in M1 phase at this temperature of 70°C. Although M2 phase appeared at this temperature in both (011) and (020)-grains, resistance continued to decrease due to the current flow through the R phase. It can be observed in both S2 and S3 that the resistance almost reached their lowest values just after M2 phase for (020)-grains disappeared. We marked temperature ranges of M2 phase for (011)-grains based on the results of Fig. 3. Even in sample S2, apparent influence of M2 phase on resistance was not recognized because the current path between two probe tips could be formed through the R phase area with a low resistivity. It is required to evaluate other physical properties such as optical reflectance and transmittance of infrared light with high spatial resolution in order to evaluate the effect of the persistent M2 phase in (011)-oriented grains. Combination of far-field infrared spectroscopy and near-field infrared microscopy will be effective for

monitoring the coexisting insulating M2 and metallic R phases through the difference in optical characteristics including optical conductivity.[45]

IV. CONCLUSIONS

Persistent M2 phase in strongly-strained (011)-oriented grains in VO_2 films grown on Al_2O_3 (001) substrates by means of conventional rf magnetron sputtering was firstly demonstrated. Temperature-dependent micro-Raman measurements showed appearance of M2 phase from 70 to 100 °C in (011)-oriented grains, in contrast to a narrower range of 10°C in (020)-oriented matrix grains. It is suggested that the appearance of M2 phase in the course of SPT of VO_2 films strongly depends on aspects of crystalline orientation and grain sizes because they dominate collective effect of stress on particular c_R-axis direction.

SUPPLEMENTARY MATERIAL

See supplementary material for the (FIG. A) Area-restricted XRD and SEM images for S3 and (FIG. B) Integrated signal intensity of M1, M2 and R phases estimated by adopting Lorentzian fittings for Raman spectra of S2 and S3.

ACKNOWLEDGMENTS

This work was supported by a Grant-in-Aid for Scientific Research (Grant No. 15K04652) from the Japan Society for the Promotion of Science.

References

[1] T. C. Chang, X. Cao, S.-H. Bao, S.-D. Ji, H.-J. Luo, and P. Jin, Adv. Manuf. **6**, 1 (2018).

[2] S. Wang, L. Kang, and D. H. Werner, Sci. Rep. **8**, 189 (2018).

[3] Y. Zou and S. Ramanathan, Proc. IEEE, **103**, 1289 (2015).

[4] Z. Yang, C. Ko, and S. Ramanathan, Annu. Rev. Mater. Res. **41**, 337 (2011).

[5] M. M. Qazilbash, M. Brehm, B-.G. Chae, P.-C. Ho, G. O. Andeev, B.-J. Kim, S. J. Yun, A. V. Balatsky, M. B. Maple, F. Keilmann, H.-T. Kim, and D. N. Basov, Science **318**, 1750 (2007).

[6] J. Sakai, J. Appl. Phys. **103**, 103708 (2008).

[7] H.-T. Kim, B.-J. Kim, S. Choi, B.-G. Chae, Y. W. Lee, T. Driscoll, M. M. Qazilbash, and D. N. Basov, J. Appl. Phys. **107**, 023702 (2010).

[8] J. Leroy, A. Crunteanu, J. Givernaud, J. C. Orlianges, C. Champeaux, and P. Blondy, Int. J. Microwave Wireless Technol. **4**, 101 (2012).

[9] G. Sun, X. Cao, X. Li, S. Bao, N. Li, M. Liang, A. Gloter, H. Gu, and P. Jin, Sol. Energ. Mat. Sol. C **161**, 70 (2017).

[10] M. A. Kats, R. Blanchard, S. Zhang, P. Genevet, C. Ko, S. Ramanathan, and F. Capasso, Phys. Rev. X **3**, 041004 (2013).

[11] K. Ito, K. Nishikawa, and H. Iizuka, Appl. Phys. Lett. **108**, 053507 (2016).

[12] N. Shukla, A. Parihar, E. Freeman, H. Paik, G. Stone, V. Narayan, H. Wen, Z. Cai, V. Gopalan, R. Engel-Herbert, D. G. Schlom, A. Raychowdhury, and S. Dutta, Sci. Rep., **4,** 4964 (2014).

[13] L. Gao, P.-Y. Chen, and S. Yu, Appl. Phys. Lett. **111**, 103503 (2017).

[14] M. Liu, H. Y. Hwang, H. Tao, A. C. Strikwerda, K. Fan, G. R. Keiser, A. J. Sternbach, K. G. West, S. Kittiwatanakul, J. Lu, S. A. Wolf, F. G. Omenetto, X. Zhang, K. A. Nelson, and R. D. Averitt, Nature **487**, 345 (2012).

[15] Y. Nakata, Y. Urade, K. Okimura, T. Nakanishi, F. Miyamaru, M. W. Takeda, and M. Kitano, Phys. Rev. Appl. **6**, 044022 (2016).

[16] Y. Muraoka and Z. Hiroi, Appl. Phys. Lett. **80**, 583 (2002).

[17] K. Nagashima, T. Yanagida, H. Tanaka, and T. Kawai, Phys. Rev. B **74**, 172106 (2006).

[18] K. Shibuya, J. Tatsumi, T. Hasegawa, and A. Sawa, Appl. Phys. Lett. **103**, 021604 (2013).

[19] M. Nakano, K. Shibuya, D. Okuyama, H. Hatano, S. Ono, M. Kawasaki, Y. Iwasa, and Y. Tokura, Nature **487**, 459 (2012).

[20] M. Marezio, D. B. McWhan, J. P. Remeika, and P. D. Dernier, Phys. Rev. B **5**, 2541 (1972).

[21] J. P. Pouget, H. Launois, T. M. Rice, P. Dernier, A. Gossard, G. Villeneuve, and P. Hagenmuller, Phys. Rev. B **10**, 1801 (1974).

[22] Y. Ji, Y. Zhang, M. Gao, Z. Yuan, Y. Xia, C. Jin, B. Tao, C. Chen, Q. Jia, and Y. Lin, Sci. Rep. **4**, 4854 (2014).

[23] S.-H. Kim, B.-J. Kim, T.-Y. Jeong, Y.-S. Lee, and K.-J. Yee, J. Appl. Phys. **117**, 163107 (2015).

[24] H. Kim, T. V. Slusar, D. Wulferding, L. Yang, J.-C. Cho, M. Lee, H. C. Choi, Y. H. Jeong, H.-T. Kim, and J. Kim, Appl. Phys Lett. **109**, 233104 (2016).

[25] M. Nazari, Y. Zhao, Z. Y. Fan, K. Ziemer, A. A. Bernussi, and M. Holtz, J Phys. D: Appl. Phys. **48**, 135101 (2015).

[26] J. I. Sohn, H. J. Joo, D. Ahn, H. H. Lee, A. E. Porter, K. Kim, D. J. Kang, and M. E. Welland, Nano Lett. **9**, 3392 (2009).

[27] S. Zhang, J. Y. Chou, and L. J. Lauhon, Nano Lett. **9**, 4527 (2009).

[28] J. Cao, Y. Gu, W. Fan, L. Q. Chen, D. F. Ogletree, K Chen, N. Tamura, M. Kunz, C. Barrett, J. Seidel, and J. Wu, Nano Lett. **10**, 2667 (2010).

[29] W. Fan, J. Cao, J. Seidel, Y. Gu, J. W. Yim, C. Barrett, K. M. Yu, J. Ji, R. Ramesh, L. Q. Chen, and J. Wu, Phys. Rev. B **83**, 235102 (2011).

[30] J. A. Atkin, S. Berweger, E. K. Chavez, M. B. Raschke, J. Cao, W. Fan, and J. Wu, Phys. Rev. B **85**, 020101(R) (2012).

[31] J. I. Sohn, H. J. Joo, K. S. Kim, H. W. Yang, A.-Rang Jang, D. Ahn, H. H. Lee, S. Cha, D. J. Kang, J. M. Kim, and M. E. Welland, Nanotechnology **23**, 205707 (2012).

[32] V. Thery, A. Boulle, A. Crunteanu, J. C. Orlianges, A. Beaumont, R. Mayer, A. mennai, F. Cosset, A. Bessaudou, and M. Fabert, Phys. Rev. B **93**, 184106 (2016).

[33] J. Jian, A. Chen, Y. Chen, X. Zhang, and H. Wang, Appl. Phys Lett. **111**, 153102 (2017).

[34] K. Okimura and J. Sakai, Jpn. J. Appl. Phys. **48**, 045504 (2009).

[35] H. Katzke, P. Toledano, and W. Depmeier, Phys. Rev. B **68**, 024109 (2003).

[36] N. H. Azhan, K. Su, K. Okimura, M. Zaghrioui, and J. Sakai, J. Appl. Phys. **117**, 245314 (2015).

[37] K. Okimura, J. Sakai, and S. Ramanathan, J. Appl. Phys. **107,** 063503 (2010).

[38] N. H. Azhan, K. Okimura, K. Matsuoka, M. Zaghrioui, and J. Sakai, J. Vac. Sci. Technol. A**35**, 061508 (2017).

[39] M. Zaghrioui, J. Sakai, N. H. Azhan, K. Su, and K. Okimura, Vib. Spectrosc. **80**, 79 (2015).

[40] Q. Luo and A. H. Jones, Surf. Coating Tech. **205**, 1403 (2010).

[41] C. Cheng, K. Liu, B. Xiang, J. Suh, and J. Wu, Appl. Phys. Lett. **100**, 103111 (2012).

[42] M.-W. Kim, W-G. Jung, H. Cho, T.-S. Bae, S.-J. Chang, J.-S. Jang, W.-K. Hong, and B.-J. Kim, Sci. Rep. **5**, 10861 (2015).

[43] J. H. Park, J. M. Coy, T. S. Kasirga, C. Huang, Z. Fei, S. Hunter, and D. H. Cobden, Nature **500**, 431 (2013).

[44] M.-W. Kim, S.-S. Ha, O. Seo, D. Y. Noh, and B.-J. kim, Nano Lett. **16**, 4074 (2016).

[45] M. M. Qazilbash, M. Brehm, G. O. Andreev, A. Frenzel, P. –C. Ho, B. –G. Chae, B. –J. Kim, S. J. Yun, H. -T. Kim, A. V. Balatsky, O. G. Shpyrko, M. B. Maple, F. Keilmann, and D. N. Basov, Phys. Rev. B **79**, 075107 (2009).

Figure Captions

FIG. 1. (a) X-ray diffraction patterns for VO_2 films with deposition time of 10, 20 and 30 min, namely S1, S2 and S3. (b) Enlarged XRD patterns for (011) peak. (c) X-ray rocking curves for (011) peak in S2 and S3.

FIG. 2. FE-SEM images for samples S1 (a), S2 (b), (c), and S3 (d). AFM image (e1) and the surface profile (e2) for S2. Backscattered electron microscopy (BSE) image (f1) and corresponding EPMA mapping for oxygen concentration (f2) for S2.

FIG. 3. Temperature-dependent micro-Raman spectra for (a) (011)-oriented and (b) (020)-oriented grains in S2. Color plots of the Raman spectra for (c) (011)-oriented and (d) (020)-oriented grains in S2. Temperature-dependent micro-Raman spectra for (e) (011)-oriented and (f) (020)-oriented grains in S3.

FIG. 4. Stress-temperature phase diagram of structural phase transition (SPT) of M1-M2-R phases for (011)-oriented grains in VO_2 films grown on Al_2O_3 (001) substrate. Stress values were calculated from the XRD peak position of diffractions from (011)-oriented grains.

FIG. 5. Resistance (R) – temperature (T) characteristics for S1, S2 and S3 films. Numerical values of derivative of resistance against temperature [$\mathrm{d}(\log_{10}R)/\mathrm{d}T$] were also plotted in upper figures in which temperature axes are common with R-T panels.

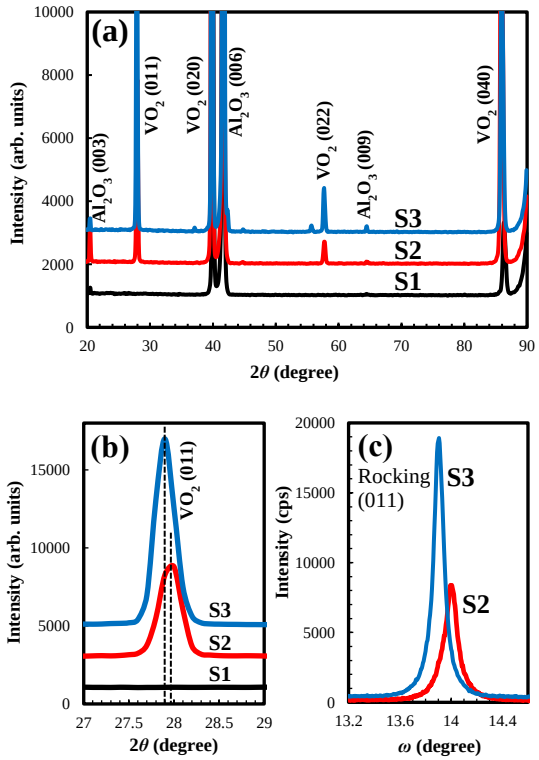

Fig. 1 K. Matsuoka *et al.*

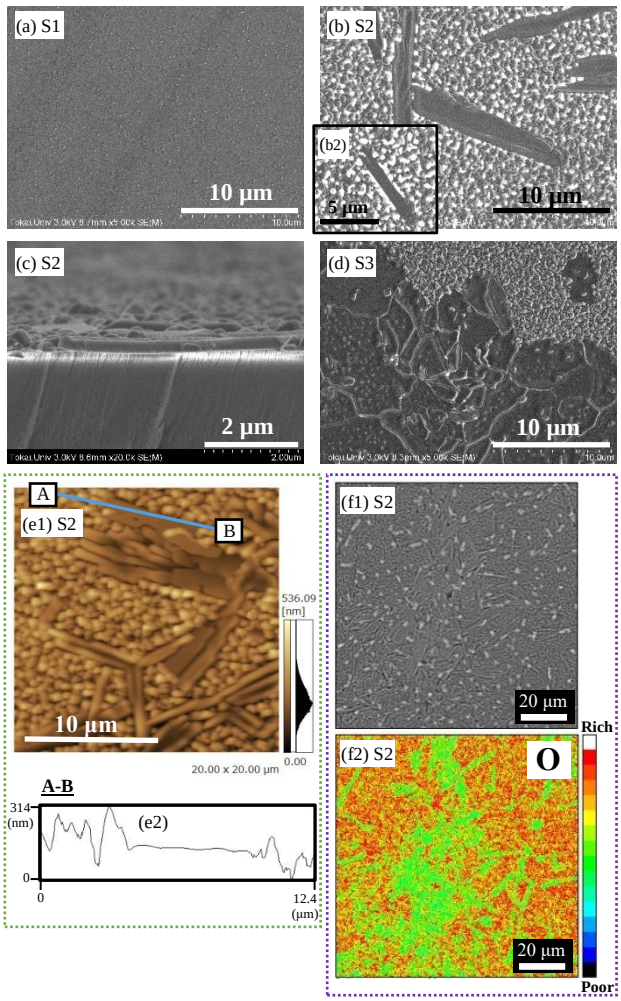

Fig. 2 K. Matsuoka *et al.*

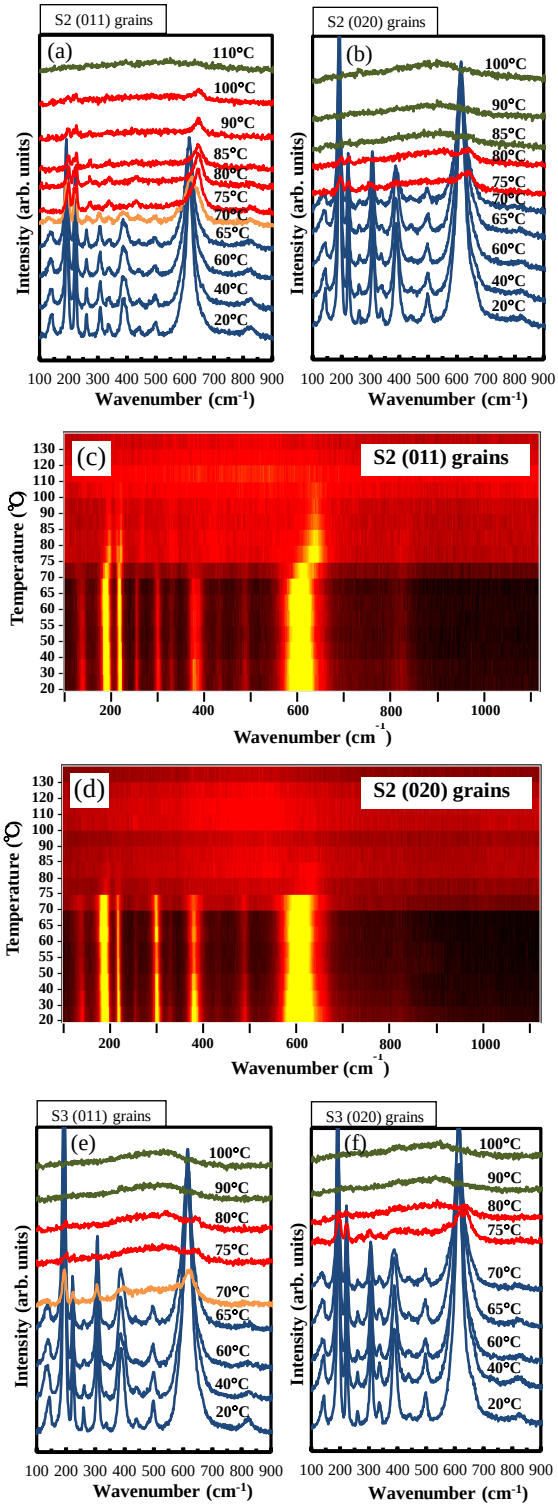

Revised Fig. 3 K. Matsuoka *et al.*

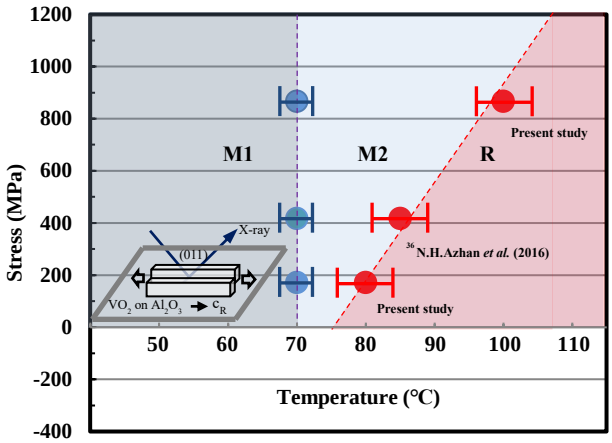

Fig. 4 K. Matsuoka *et al.*

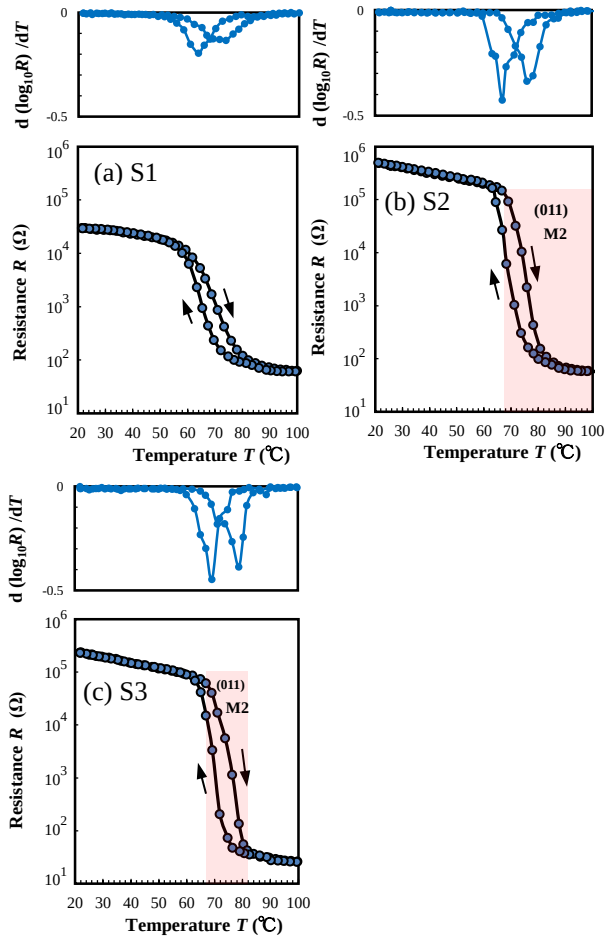

Revised Fig. 5 K. Matsuoka *et al.*